THE JOURNAL OF PHYSICAL CHEMISTRY C

Article

Characterizing Electron-Hole Plasma Dynamics at Different Points in Individual ZnO Rods

Ralph L. House, Justin R. Kirschbrown, Brian P. Mehl, Michelle M Gabriel, Joseph A Puccio, James K Parker, and John Michael Papanikolas

J. Phys. Chem. C, **Just Accepted Manuscript** • Publication Date (Web): 22 September 2011

Characterizing Electron-Hole Plasma Dynamics at Different Points in Individual ZnO Rods

*Ralph L. House, Justin R. Kirschbrown, Brian P. Mehl, Michelle M. Gabriel, Joseph A. Puccio, James K. Parker[1] and John M. Papanikolas**

Department of Chemistry, Caudill Laboratories, University of North Carolina at Chapel Hill, Chapel Hill, North Carolina 27599

*** Author to whom correspondence should be addressed.**

john_papanikolas@unc.edu

RECEIVED DATE ()

ABSTRACT: We have used two-photon emission microscopy to characterize the charge carrier dynamics at different locations within a single ZnO rod. Photoexcitation by a focused laser produces carriers (electrons and holes) in a localized region. Emission is detected using both time-integrated and time-resolved methods. Results show that the electron-hole plasma (EHP) state plays a larger role at the end of the rod compared to other points within the structure, where electron-hole recombination proceeds through an excitonic state. The origin of this spatial dependence is attributed to the physical confinement at the end of the structure that prevents an expansion of the photoexcited electron-hole cloud through processes such as carrier diffusion. Whispering gallery modes are identified as contributing to a periodic emission pattern along the length of the structure.

[1] Chemical Sciences Division, U.S. Army Research Office, PO Box 12211, Research Triangle Park, NC 27709

KEYWORDS: Zinc Oxide, Electron-Hole Plasma, time-resolved emission, two-photon emission microscopy, ultrafast dynamics

I. INTRODUCTION

At low excitation intensities the optical properties of semiconductors are determined by single electron-hole pairs that exist either in excitonic states or as free carriers in the continuum. As the excitation intensity and corresponding carrier density increase, the separation between excitons becomes comparable to, or smaller than, the Bohr radius. The charge carrier interactions that emerge in this high-density regime give rise to a host of nonlinear optical effects, including a weakening of the exciton binding due to Coulombic screening, and ultimately the formation of a collective electron-hole plasma (EHP) phase. The many-body exchange and correlation interactions that are present in the EHP stabilize the photoexcited state, resulting in a narrowing of the band-gap that is often referred to as band-gap renormalization.[1] Furthermore, the oscillator strength is enhanced in the EHP, and electron-hole recombination in this high density limit is characterized by an intense, red-shifted emission compared to its excitonic counterpart.[2]

Finite-sized structures offer an additional layer of complexity and opportunity. When an object's dimensions are comparable to the wavelength, its size and shape play a central role in determining its optical properties. The shape of the object can give rise to complex cavity resonances that concentrate the optical field in specific locations, becoming an intrinsic part of the optical response. While most examples of cavity resonances have come from engineered systems, similar effects are possible in nanoscale and mesoscale structures.[3-10]

Electron-hole plasma formation has been observed in bulk materials and single nanostructured objects. However, the potential for EHP variation across different regions within a single structure, and the relation between EHP formation and local optical cavity modes, has not been explored. Here we describe the use of two-photon emission microscopy to examine the spatial variation in EHP formation in individual needle-shaped ZnO rods and relate EHP formation with local optical cavity modes. The combination of facile EHP formation in ZnO[6-9,11,12] and the diverse set of synthetically available crystalline structures with complex geometrical architectures[13-15] make this an ideal material for

investigating shape dependent EHP formation. Previous work in our lab investigated the excited state dynamics of needle-shaped ZnO rods with spatial specificity.[16-19] This report builds upon that work by examining the EHP dynamics in different regions of individual rods (e.g. end vs. middle) using both time-integrated and time-resolved methods. Experiments using a focused laser beam to excite a spatially localized region of the rod show a greater propensity for EHP formation in the narrow tips compared to the interior regions where the rod's cross section is larger. We attribute this spatial variation to a physical confinement of carriers that inhibits expansion of the charge cloud at the end the structure, maintaining the density of electron-hole pairs and the EHP state. In addition to the spatial variation in EHP formation, the optical properties are strongly influenced by whispering gallery (WG) modes supported within the rod's hexagonal cross-section. It is the combination of spatially varying EHP and optical cavity modes that give rise to the complex emission images and spatially heterogeneous behavior.

2. EXPERIMENTAL

Studying the carrier dynamics at different points within a single structure necessitates a technique with high temporal resolution and spatially localized excitation. The microscope used here combines an ultrafast laser source with a home-built inverted microscope.[18] Two photon excitation is achieved using the 730 nm output of a mode-locked (80 MHz) Ti:Sapphire laser. Light from the laser is directed through a prism-pair compressor and reflected off a dichroic beam splitter (R: 680-1000 nm, T: 360-650 nm) onto the back aperture of the objective (Olympus MSPlan 50x, 0.8 NA), which focuses the beam to a diffraction limited spot. Because two-photon excitation scales with the square of the laser intensity, the lateral dimension of the excitation is approximately 350 nm. Photoluminescence collected by the objective passes through the beam-splitter, and is directed into a monochromator and detected by a photomultiplier tube for time integrated measurements, or a streak camera for time-resolved detection (~10 ps time resolution). Imaging is achieved by raster-scanning the sample across the focal point of the

objective using a piezo-electric stage (Queensgate NPS3330 Controller/Stage System).

The structures were synthesized using hydrothermal techniques, drop-cast onto a glass microscope slide and annealed at 550 ^{O}C prior to study. Through the course of this study we examined approximately 10 needle-shaped rods. The scanning electron microscopy (SEM) image of a typical structure is shown on the right of Figure 1A. While there is some variation in size, the structures are all crystalline, with faceted, hexagonal cross-sections. They generally vary between 10-20 μm in length and are 1-2 μm in diameter at the middle, tapering down to ~300-500 nm at the ends.

3. RESULTS AND DISCUSSION

Zinc oxide is a wide band gap semiconductor (3.37 eV) with a strong exciton binding energy (60 meV).[13,15] Photoexcitation in the ultraviolet, or two-photon excitation in the near infrared, promotes electrons from the valence band to the conduction band. The free carriers that are produced can relax into excitons (at low excitation intensities), resulting in a near-UV emission at 390 nm, or become trapped at defect sites giving rise to a broad visible emission centered at 550 nm.

Imaging: Two-photon microscopy images obtained by monitoring the band edge (390 nm) and trap (550 nm) emission channels following two-photon excitation at 730 nm of a typical rod (denoted **R1**) are shown along with the SEM image in Figure 1. The increased areas of intensity at the ends of the structure are a particularly prominent feature in both the band-edge and trap emission images. A closer comparison of the two images, however, shows that the bright spots are slightly offset, with the trap image showing its most intense emission slightly to the left of the band-edge. This shift is likely a consequence of the roughness observed at the tip of this rod, which would result in a greater defect density and brighter trap emission.

Optical Cavity Modes: In addition to the bright ends, the emission from the interior of the rod is

periodically modulated and appears to coincide with the facets in both the trap and band-edge emission images, with greater contrast in the band-edge. Not every rod exhibits a pattern of this nature, but most do, and the contrast in the band-edge image is generally always greater. This spatial variation most likely results from the influence of optical cavity modes (supported by the rod's hexagonal cross section) on the emission intensity. Generally, there are two types of modes – standing wave (Fabry-Perot, FP) resonances that are supported between two parallel facets, and whispering gallery (WG) modes that correspond to propagation of light around the periphery of the hexagonal cross-section through total internal reflection off each facet. We previously identified the influence of FP and WG modes on second-harmonic generation in ZnO rods,[17] and WG modes have been implicated in a number of other spectroscopic measurements of ZnO structures.[20-25] The coincidence of the bright spots in the emission images with the vertices of the hexagonal facets suggests that it is the WG modes that influence photoluminescence in these structures.

For a given wavelength, λ, the resonance condition dictates that modes will be supported for specific cross-sectional diameters of the rod, i.e.

$$d_m = \frac{\lambda}{3n}\left[m + \frac{6}{\pi}\tan^{-1}(\beta\sqrt{3n^2-4}) \right] \quad (1)$$

where d is the separation between two parallel facets and m is an integer that specifies the mode number.[22,26] In this expression n is the refractive index and β depends upon the polarization of the light. The spacing between adjacent modes, $\Delta d = d_{m+1} - d_m$ is then $\lambda/3n$.

The periodic nature of the emission pattern in the tapered structure arises because the facet spacing changes along the length of the rod.[17] Analysis of the SEM images for this rod show that the facet separation varies nearly linearly with distance along the rod, resulting in a series of resonances observed along the structure that are spaced by:

$$\Delta L = \frac{\Delta d}{\alpha} = \cdot\frac{\lambda}{3n\alpha} \quad (2)$$

where α is the change in the facet spacing per unit length along the rod. For the rod shown in Figure 1,

α = 120 nm/μm in the vicinity of the resonances.

The WG modes can influence the emission either through spatial modulation of the excitation or enhancement of the photoluminescence through constructive interference. Using λ = 730 nm and n=2 in the above expression yields a predicted spacing, ΔL, between optical resonances of approximately 0.9-1.0 μm, which is close to the observed spacing of 1.0-1.1 μm. This suggests that the periodic variation observed in the emission images arises (at least in part) from excitation light coupling into the WG modes, resulting in a concentration of the optical field at specific locations within the rod and regions of localized excitation. In addition to the excitation light, a coupling of the 390 nm emission into the WG resonator may also play a role. While the predicted spacing for adjacent resonances (m, m+1) in the band-edge emission (390 nm) is only 0.5 μm, too small to account for the observed pattern, the spacing between alternating resonances (m, m+2) would also be around 1.0 μm. Thus, the periodic pattern observed in the band-edge emission image may stem from a situation in which *both* the excitation and emission light are quasi-resonant. This double resonance condition is not expected to be present in the trap image, where the resonance condition cannot be simultaneously satisfied by the 730 nm excitation light and the 550 nm defect emission, accounting for the lesser degree of contrast observed in the defect emission image.

Spatially Dependent EHP Formation: Spectroscopic measurements are performed by positioning the excitation spot at specific points in the structure. The photoluminescence spectra shown in Figure 1B were collected from the end of the rod and at a point located between the end and middle, denoted interior. (Note throughout this manuscript the 'end of the rod' refers to the location of the bright point in the band-edge emission image.) Emission spectra observed at different locations have the same spectral features, namely a narrow transition centered ~390 nm that corresponds to electron-hole recombination from the band-edge (BE) and a broad trap emission band at ~550 nm (T). While the spectra have the same basic form, the intensity of the band-edge emission relative to the trap depends on the position in

the structure, with the spectrum obtained from the end exhibiting a greater BE:T intensity ratio than the interior (~20:1 vs. ~5:1). The spatial variation in the BE:T ratio is one indicator that photophysics at the end of the structure differ markedly from those in the interior.

The band-edge emission spectrum at the end of the rod also shows a significant dependence on excitation intensity relative to other points. Band-edge emission spectra collected at different excitation intensities are show in Figure 2 for three different locations in two different rods, **R1** and **R2**. Dashed circles on two-photon emission images that accompany each set of spectra indicate the locations where the spectra were collected. At the middle of the rod, the spectra are independent of excitation intensity, with $\lambda_{max} \approx 390$ nm. On the other hand, at the end of the rod, the spectra systematically shift to lower energy with increasing excitation energy. In the case of **R2**, a broadening of the spectrum is also observed; however, the degree to which this happens varies from rod to rod. Similar, but less dramatic changes, are observed in the interior. We have observed this phenomenon to differing degrees in multiple structures. A systematic examination of 9 rods shows that on average there is an 8 nm shift at the end, a 4 nm shift in the interior and a 2 nm shift in the middle of the structure.

The red-shift in the emission band is consistent with the formation of an EHP at higher excitation intensities.[8-10,27] At low excitation intensity the band-edge (BE) emission arises predominantly from exciton recombination. As the carrier density increases, Coulombic screening weakens the exciton binding energy, resulting in dissociation of the electron-hole pairs and the transition to the EHP state. Experimental gain spectra suggest the transition to the EHP in ZnO occurs at carrier densities between 10^{17} and 10^{19} cm^{-3}.[1] Based on the two-photon cross section for ZnO and excitation intensities used here, we estimate that each laser pulse produces a charge carrier density of $\approx 10^{21}$ cm^{-3}.[28]

The many-body correlation and exchange interactions between carriers that are present in the high density EHP regime alter the electronic structure of the semiconductor. Because the Pauli principle forbids electrons with parallel spin to occupy the same unit cell, the distance between electrons increases, reducing the Coulombic repulsion. There is also a greater probability of finding an electron

near a hole (and vice versa) than finding two like charges in the same vicinity, and the two effects combined lower the total energy of the system.[1] The net result of this stabilization of the plasma is a monotonic decrease of the band gap with increasing electron-hole pair density. As a consequence, the emission spectrum resembles the exciton emission at low laser power, but shifts to the red as the excitation intensity increases and the system transitions to an EHP state.

Closer inspection of the spectra shows that at the lowest excitation intensity the spectra at the end of the structure exhibit some differences relative to their counterparts in the interior. The **R1** spectrum is slightly blue shifted and the **R2** spectrum is broadened. While the broadening is suggestive of the beginnings of plasma formation, the blue shift is consistent with the weakening of the exciton that occurs as their Bohr orbits begin to overlap.[1] These differences indicate that the photophysics at the end of the structure are influenced by carrier-carrier interactions, even at the lowest excitation intensities.

The dependence of the spectrum on carrier density implies that the EHP emission should have a distinct temporal signature, showing an emission spectrum that appears initially to the red of the exciton band and shifts to the blue with time as electrons and holes recombine and the carrier density drops. The spectral-temporal intensity map in Figure 3A depicts the evolution of the BE emission following 17 mW excitation at the end of the rod labeled **R3**. The fluorescence image of this rod is shown in the inset of Figure 3A. Spectra at specific times can be obtained by taking horizontal slices across the intensity map. A comparison of spectra extracted at 0, 80 and 200 ps show that the spectra shift to higher energy over the first 200 ps following photoexcitation (Figure 3B), consistent with the instantaneous appearance of an EHP and a subsequent transition to an excitonic state. When the experiment is conducted in the same region of the rod with a lower power (5 mW), the shift in the spectrum disappears (Figure 3C), in line with the formation of an excitonic state.

In the smaller regions at the ends of the structure, we observe an increase in the magnitude of the spectral red shift (Figure 2), consistent with the formation of an EHP. The implication is that the photogenerated carriers in these locations must have a density that is high enough to support transition

of the nascent charge distribution to the EHP. This is greatly facilitated at the end of the structure where physical confinement of the charge carriers will help to maintain the close interaction. In the middle of the structure carriers can migrate away from the excitation region, either through simple diffusion, or perhaps driven by internal fields that separate the electrons and holes. Based on the carrier diffusion constant in ZnO (~10 cm^2 s^{-1}),[29,30] we estimate a field-free diffusion length of ≈300 nm during the first 100 ps after excitation. Band-bending in ZnO is anticipated to result in electric fields and a depletion zone that extends a hundred nanometers or more into the bulk, which could increase this even further. The net result is a decrease in the charge density that makes it more difficult to form and sustain the EHP. As a result, the emission observed at the interior locations arises predominantly from excitonic recombination.

The transition from the excitonic state to the EHP is also accompanied by characteristic changes in the emission intensity. A decrease in the oscillator strength of the exciton emission is expected as the carrier density increases. In this intermediate regime, the exciton-exciton interactions result in a weakening of the exciton binding energy that is accompanied by an increase in the excitonic radius and a corresponding decrease in the overlap of the electron and hole wavefunctions. This trend reverses as the system transitions from this intermediate regime to the EHP, where an increased correlation between the electrons and holes results in a greater oscillator strength (i.e. excitonic enhancement), and a brighter emission than its exciton counterpart.[2] This increase in oscillator strength could explain the more intense band-edge emission observed both in the images and in the spectra collected at the ends of the structure.

Shown in Figure 4 is the intensity of the band-edge and trap emission as a function of the square of the laser power at three different points located along the central axis of **R1**. The trap emission exhibits a linear increase in this representation, indicating that it is simply proportional to the carrier density produced by two-photon excitation. The band-edge emission on the other hand shows upward curvature, signifying that its intensity increases super-linearly with the carrier density. This upward curvature is more pronounced at the end of the rod, where the red shift in the emission spectrum shows

the contribution from the EHP is greatest. The intensity dependence of the BE emission (both its intensity and spectral position) indicates a spatially dependent propensity for EHP formation, with the degree of correlation and exchange interactions increasing (i.e. greater degree of EHP) as the excitation is moved from the middle to the end of the rod.

Whispering Gallery Mode Stimulated Emission. One signature of stimulated emission in ZnO is an increase in the ratio of the band-edge to trap emission intensities with increasing laser power. Shown below the plot in Figure 4 are images of the BE:T ratio at two different laser powers. At low laser powers there is a generally uniform BE:T ratio of ≈2 observed throughout the interior of this rod, and a localized region of ≈12-13 at the end. Given the small excitation volume at this location, we anticipate that spontaneous EHP emission is the main contributor to the total emission and that the increase in the BE:T ratio is due primarily to the EHP oscillator strength. However, because of its large oscillator strength, EHP emission in ZnO is often associated with stimulated emission and lasing in finite sized structures,[7-9,11,12,25,31-35] and as a result it is difficult based on our data alone to rule out contributions from stimulated emission at the end of the rod. It is interesting to note that the BE:T ratio is ≈0.5-0.7 at the very tip of the rod, where the most intense spot in the trap emission image occurs, highlighting the greater influence of the trap emission where the structure terminates. Our focus, however, is not on the end of the structure but on the changes that occur in the interior.

In the rod's interior, the BE:T ratio grows by a factor of 30-40 as the laser power is increased from 5 to 17 mW; however, the growth is not uniform across the structure. The WG mode pattern is more pronounced in the BE:T ratio image at the higher power, indicating that resonance locations exhibit a disproportionate increase in the band-edge emission intensity. This is evident in the band-edge images themselves, which are shown at low and high excitation intensities in Figure 5. The emission intensity along the length of the rod is displayed in the right-hand panel, which shows the integrated signal across a row of pixels as a function of longitudinal position. As the laser power is increased, the brightness of

the interior WG modes exceeds even that observed at end of the rod.

These observations must arise from a situation in which the rod's cross-sectional diameter also supports a WG resonance at 390 nm. Under these circumstances, emission (exciton or EHP) from the excitation region would travel around the periphery of the rod undergoing total-internal reflection at each facet resulting in stimulated emission. Because we do not see a narrowing of the emission spectrum (Figure 2D-2F), which would be an indicator of WG mode lasing, the enhancement of the mode pattern observed here is probably better described by amplified spontaneous emission.

Closer inspection of the images shows that for a given WG mode, the emission intensity depends upon the lateral position of the excitation. Figure 6 shows this variation for one of the WG resonances in **R1**, where the expanded view in the figure corresponds to the area indicated by the red rectangle in Figure 5. The intensity profile across the rod (right-hand side of panel) shows two peaks that coincide with the outer facets of the structure. Comparison of lateral profiles taken at different powers shows that the contrast depends upon laser intensity, with the peaks increasing more than the interior. Intensity dependence measurements performed at the "bright" and "dim" spots marked on the image are displayed in Figure 6B. The brighter spot shows a steeper increase in the emission intensity with increasing pulse energy.

The lateral variation in the intensity dependence is indicative of a non-linear optical effect, either in the degree of excitation or in the enhancement of the stimulated emission. One possibility is that the WG mode results in an enhancement in the optical field, which in turn leads to a greater carrier density and a more intense EHP. This does not appear to be the case, however, as the two locations (Figure 6C and 6D) show similar power-dependent spectral shifts, implying similar EHP characteristics. A more likely possibility for its origin lies in the positional differences of the excitation. When the rod is excited near its edge, light emitted by the electron-hole recombination event will be better positioned to undergo total internal reflection and travel around the periphery of the rod, stimulating emission on each successive round trip. The splitting of the WG resonance into two spots may be a consequence of a

better coupling of the emission into the WG mode at those locations.

4. CONCLUSIONS

We have implemented two-photon emission microscopy to locally excite different regions of individual ZnO rods at steadily increasing excitation intensities. Results from steady-state spectral analyses show that the BE emission band shifts to lower energy with increasing excitation power at the end of the rod. The magnitude of the shift is greatly diminished in the rod interior (by a factor of two on average) and disappears almost completely in the middle. These observations are consistent with the preferential formation of an EHP at the end of the rod. Time-resolved emission data confirms this notion, showing a time-dependent spectral blue shift in the band edge emission when the end of the rod is excited with high power. This corresponds to disappearance of the EHP and subsequent recovery of the band-gap. No shift is observed at low excitation intensities. Images obtained under high power conditions show a pronounced whispering gallery (WG) mode pattern that enhances the stimulated emission. Collectively, our results show that different regions of a single structure can exhibit distinctly different photophysical behaviors.

ACKNOWLEDGMENT: Support for RLH, JRK and BPM was provided by a grant from the National Science Foundation (CHE-0809045). Support for MMG during the latter stages of the project was provided by a grant from the U. S. Army Research Laboratory and the U. S. Army Research Office under contract number W911NF-04-D-0004. The project also made use of instrumentation purchased by the UNC-EFRC on Solar Fuels and Next Generation Photovoltaics, an Energy Frontier Research Center funded by the U.S. Department of Energy, Office of Science, Office of Basic Energy Sciences under Award Number DE-SC0001011.

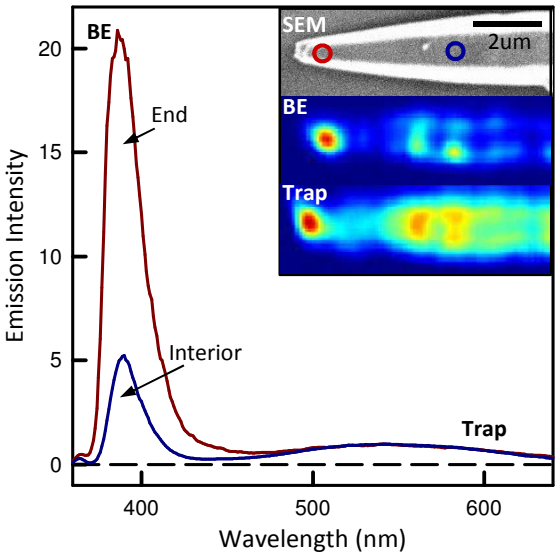

Figure 1: Band-edge (BE) and Trap (T) emission images of the rod shown in the SEM image. The rods are needle-shaped and symmetric, although in this image only the left-hand side of the structure is shown. The fluorescence images were obtained at a laser power of 10 mW and show increased intensity at the end of the rod and modulated intensity throughout the interior. Emission spectra collected by positioning the excitation spot at the end (red) and interior (blue) of the structure show two bands arising from band-edge emission (BE) at 400 nm and trap recombination at 550 nm. The locations of the spectra are indicated by the colored circles in the SEM image.

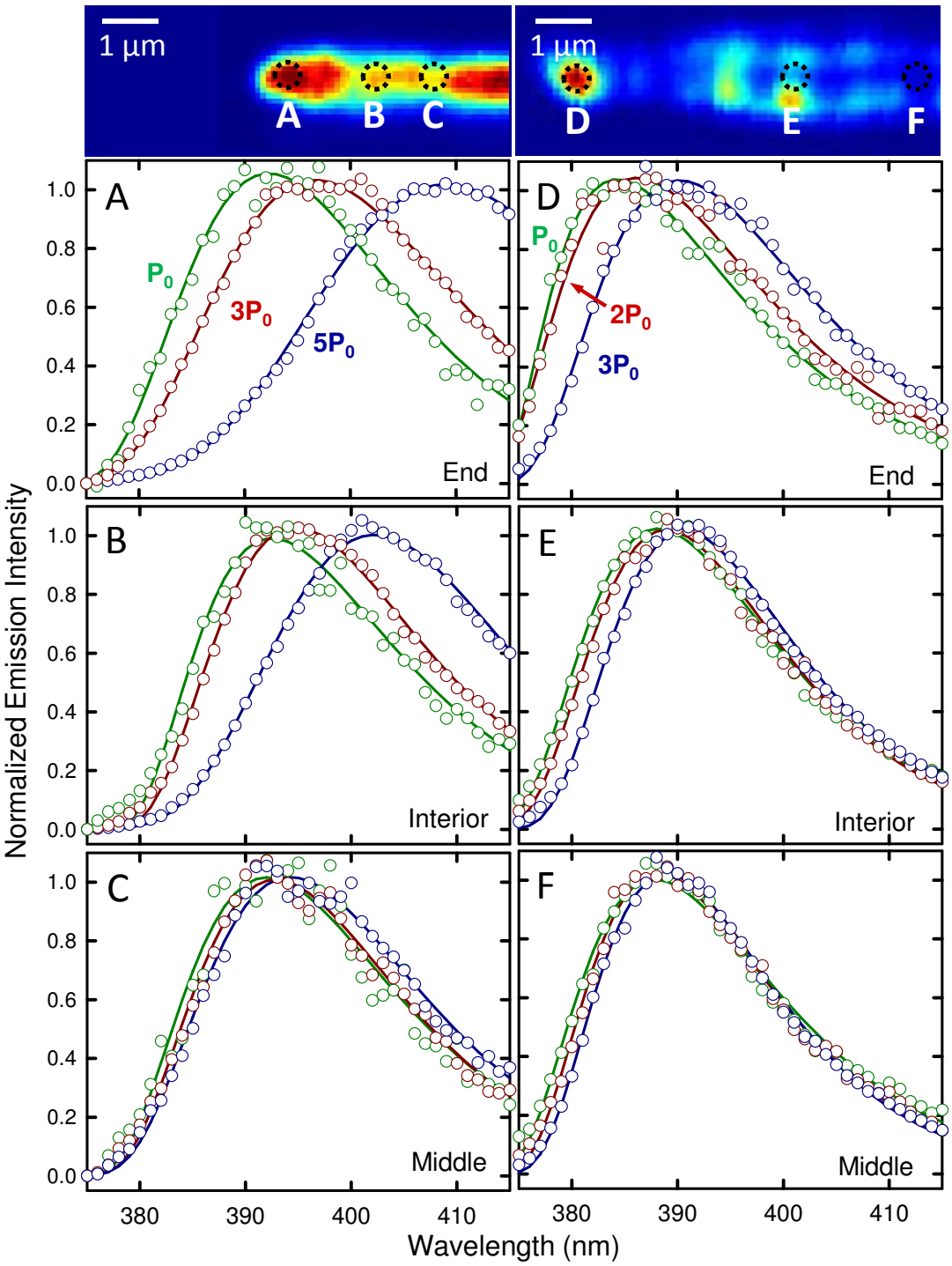

Figure 2: Band-edge emission spectra collected at a series of laser powers at three different points within two different structures, **R1** and **R2**. Emission images for the two structures are shown at the top. Panels (A-C) and the left-hand image correspond to **R2**, panels (D-F) and right-hand image **R1**. The scale bar in both images is 1 µm. The locations marked A-F indicate the points at which the spectra shown in panels A-F were collected. Each panel shows three spectra collected using low (green), intermediate (red) and high (blue) laser power. The green spectra in panels A-C were collected at the same power (P_0), as were the red ($3P_0$) and blue ($5P_0$). The same is true for panels D-F, but green, red and blue correspond to P_0, $2P_0$ and $3P_0$. In both cases P_0 = 5 mW.

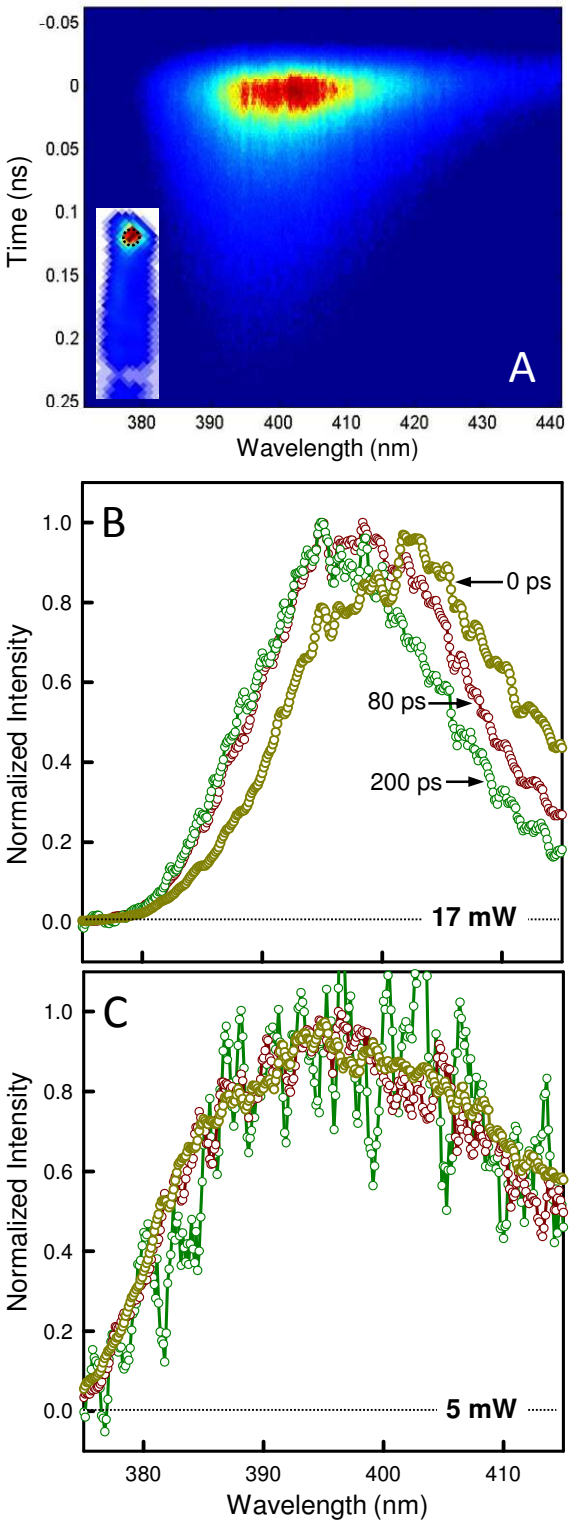

Figure 3: Time-resolved emission data collected from the end of structure **R3**. (A) Intensity map depicting emission as a function of time and wavelength (blue corresponds to low intensity, red high intensity) obtained under high laser power conditions (17 mW). Inset show emission image. (B) Emission spectra obtained by taking horizontal slices through this emission map at 0 ps (gold), 80 ps (red) and 200 ps (green) after excitation show a time-dependent blue shift of the band. (C) Emission

spectra collected from the same point, but at a lower laser power (5 mW), show no shift.

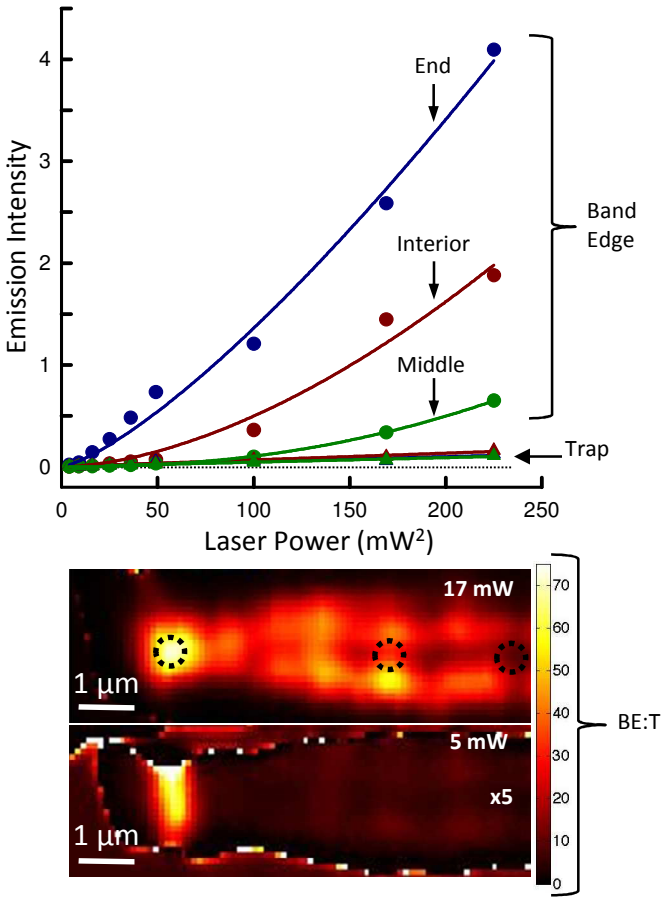

Figure 4. Intensities of the band-edge and trap emission bands in **R1** as a function of laser power at the end (blue), interior (red) and middle (green). The three locations are indicated by the points labeled D, E and F, respectively, in the right-hand image of Figure 2. Images represent the BE:T ratios obtained by dividing the band-edge image by the trap image at two different laser powers. The 5 mW image was multiplied by a factor of 5, and shares the same scale bar as the 17 mW image. The scale bar in the image is 1 µm.

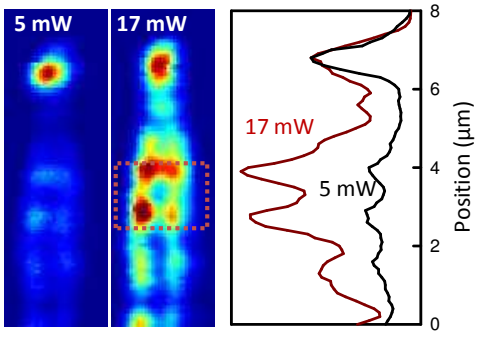

Figure 5: Band-edge emission images of **R1** obtained under low power (5 mW) and high power (17 mW) conditions. The images are scaled to have the same intensity at the end of the rod. The images are 8 μm in vertical dimension. Right-hand panel shows the emission intensity (obtained by summing the intensity across a row of pixels) along the longitudinal axis of the rod for the two different powers. The WG mode pattern becomes more pronounced at higher powers.

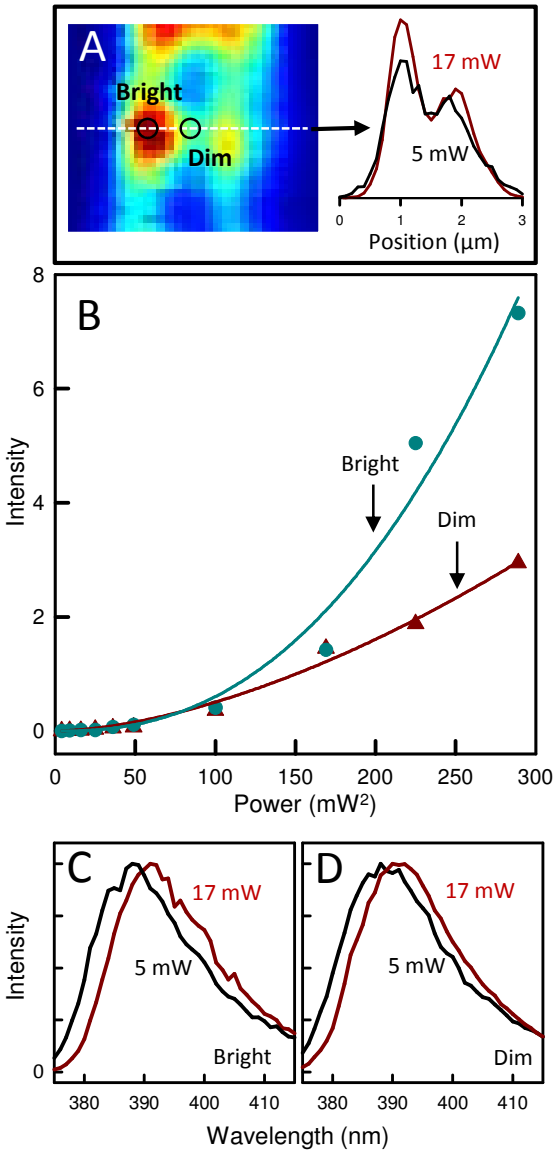

Figure 6: (A) Expanded image of the WG mode in **R1** indicated by the red rectangle in Figure 5. The horizontal dimension of the image is 3 μm. The profile at the right corresponds to a horizontal cut along the dotted line in the image for both the low (5 mW) and high (17 mW) power cases. (B) The intensity of the band-edge emission at the two points along this line that are labeled 'bright' and 'dim' in the image. (C) and (D) are the band-edge emission spectra collected from these two point at low (5 mW) and high (17 mW).

REFERENCES:

(1) Klingshirn, C. F. *Semiconductor optics*, 3rd ed.; Springer: Berlin ; New York, 2007.

(2) Pavesi, L.; Staehli, J. L.; Capozzi, V. *Solid State Commun.* **1987**, *61*, 321.

(3) Voss, T.; Svacha, G. T.; Mazur, E.; Muller, S.; Ronning, C.; Konjhodzic, D.; Marlow, F. *Nano Lett.* **2007**, *7*, 3675.

(4) Sun, L. X.; Chen, Z. H.; Ren, Q. J.; Yu, K.; Bai, L. H.; Zhou, W. H.; Xiong, H.; Zhu, Z. Q.; Shen, X. C. *Phys. Rev. Lett.* **2008**, *100*, 156403.

(5) van Vugt, L. K.; Ruhle, S.; Ravindran, P.; Gerritsen, H. C.; Kuipers, L.; Vanmaekelbergh, D. *Phys. Rev. Lett.* **2006**, *97*, 147401.

(6) Johnson, J. C.; Yan, H. Q.; Schaller, R. D.; Petersen, P. B.; Yang, P. D.; Saykally, R. J. *Nano Lett.* **2002**, *2*, 279.

(7) Song, J. K.; Willer, U.; Szarko, J. M.; Leone, S. R.; Li, S.; Zhao, Y. *J. Phys. Chem. C* **2008**, *112*, 1679.

(8) Leung, Y. H.; Kwok, W. M.; Djurisic, A. B.; Phillips, D. L.; Chan, W. K. *Nanotechnology* **2005**, *16*, 579.

(9) Takeda, J.; Kurita, S.; Chen, Y. F.; Yao, T. F. *Int. J. Mod Phys B* **2001**, *15*, 3669.

(10) Zu, P.; Tang, Z. K.; Wong, G. K. L.; Kawasaki, M.; Ohtomo, A.; Koinuma, H.; Segawa, Y. *Solid State Commun.* **1997**, *103*, 459.

(11) Song, J. K.; Szarko, J. M.; Leone, S. R.; Li, S. H.; Zhao, Y. P. *J. Phys. Chem. B* **2005**, *109*, 15749.

(12) Szarko, J. M.; Song, J. K.; Blackledge, C. W.; Swart, I.; Leone, S. R.; Li, S. H.; Zhao, Y. P. *Chem. Phys. Lett.* **2005**, *404*, 171.

(13) Djurisic, A. B.; Leung, Y. H. *Small* **2006**, *2*, 944.

(14) Wang, Z. L. *Journal of Physics-Condensed Matter* **2004**, *16*, R829.

(15) Ozgur, U.; Alivov, Y. I.; Liu, C.; Teke, A.; Reshchikov, M. A.; Dogan, S.; Avrutin, V.; Cho, S. J.; Morkoc, H. *J. Appl. Phys.* **2005**, *98*, 041301.

(16) Mehl, B. P.; Kirschbrown, J. R.; House, R. L.; Papanikolas, J. M. *Journal of Physical Chemistry Letters* **2011**, *2*, 1777.

(17) Mehl, B. P.; House, R. L.; Uppal, A.; Reams, A. J.; Zhang, C.; Kirschbrown, J. R.; Papanikolas, J. M. *J. Phys. Chem. A* **2010**, *114*, 1241.

(18) House, R. L.; Mehl, B. P.; Kirschbrown, J. R.; Barnes, S. C.; Papanikolas, J. M. *J. Phys. Chem. C* **2011**, *115*, 10806.

(19) House, R. L.; Mehl, B. P.; Zhang, C.; Kirschbrown, J. R.; Barnes, S. C.; Papanikolas, J. M. *Proceedings of the SPIE* **2009**, *7396*, 73960G.

(20) Liu, J. Z.; Lee, S.; Ahn, Y. H.; Park, J. Y.; Koh, K. H.; Park, K. H. *Appl. Phys. Lett.* **2008**, *92*, 263102.

(21) Nobis, T.; Grundmann, M. *Phys Rev A* **2005**, *72*, 063806.

(22) Nobis, T.; Kaidashev, E. M.; Rahm, A.; Lorenz, M.; Grundmann, M. *Phys. Rev. Lett.* **2004**, *93*, 103903.

(23) Czekalla, C.; Sturm, C.; Schmidt-Grund, R.; Cao, B. Q.; Lorenz, M.; Grundmann, M. *Appl. Phys. Lett.* **2008**, *92*, 241102.

(24) Zhang, Y.; Zhou, H. J.; Liu, S. W.; Tian, Z. R.; Xiao, M. *Nano Lett.* **2009**, *9*, 2109.

(25) Dai, J.; Xu, C. X.; Wu, P.; Guo, J. Y.; Li, Z. H.; Shi, Z. L. *Appl. Phys. Lett.* **2010**, *97*.

(26) Grundmann, M.; Czekalla, C.; Nobis, T.; Rahm, A.; Cao, B. Q.; Zuniga-Perez, J.; Sturm, C.; Schmidt-Grund, R.; Lorenz, M. *Phys Status Solidi B* **2010**, *247*, 1282.

(27) Cheng, B. C.; Yu, X. M.; Liu, H. J.; Fang, M.; Zhang, L. D. *J. Appl. Phys.* **2009**, *105*.

(28) Lin, J. H.; Chen, Y. J.; Lin, H. Y.; Hsieh, W. F. *J. Appl. Phys.* **2005**, *97*, 033526.

(29) Mitsubori, S.; Katayama, I.; Lee, S. H.; Yao, T.; Takeda, J. *Journal of Physics-Condensed Matter* **2009**, *21*.

(30) Takeda, J.; Takagi, K.; Okabe, T.; Ko, H. J.; Yao, T. *Physica Status Solidi* **2004**, *1*, 678.

(31) Johnson, J. C.; Yan, H. Q.; Yang, P. D.; Saykally, R. J. *J. Phys. Chem. B* **2003**, *107*, 8816.

(32) Yang, P. D.; Gargas, D. J.; Moore, M. C.; Ni, A.; Chang, S. W.; Zhang, Z. Y.; Chuang, S. L. *Acs Nano* **2010**, *4*, 3270.

(33) Kalt, H.; Fallert, J.; Dietz, R. J. B.; Sartor, J.; Schneider, D.; Klingshirn, C. *Phys Status Solidi B* **2010**, *247*, 1448.

(34) Anastasiadis, S. H.; Stassinopoulos, A.; Das, R. N.; Giannelis, E. P.; Anglos, D. *J Opt-Uk* **2010**, *12*.

(35) Shih, T.; Mazur, E.; Richters, J. P.; Gutowski, J.; Voss, T. *J. Appl. Phys.* **2011**, *109*.

TOC IMAGE: